АНТЕНЕ И ПРОСТИРАЊЕ
/
ANTENNAS AND PROPAGATION

(АП/APl)

Karakteristike materijala za štampane antene u opsegu 65-110 GHz

Nikola Bošković i Miloš Radovanović

***Apstrakt*—Izbor materijala igra presudnu ulogu u karakteristikama štampanih antena. Ovo je naročito kritično na W- opsegu, gde je mehanizam gubitaka značajno izmenjen, zbog čega veoma mali broj standardnih dielektrika može biti korišćen. Radi suzbijanja parazitnih modova i površinskih talasa, debljina dielektrika mora biti veoma mala u odnosu na učestanost, što dovodi do toga da efekat površinske hrapavosti bakarne provodne folije ima dominantan uticaj na gubitke. U ovom radu je prikazan značaj izbora odgovarajuće folije kao i njen uticaj. Zaključci su praćeni simulacijama i merenjima.**

***Ključne reči*—Balansni mikrostrip, gubici u materijalu, štampana tehnologija, štampane antene.**

I. UVOD

Štampane antene su klasa antena koje se tipično sastoji od provodnika koji je najčešće u vidu tanke bakarne folije, i dielektrika na kome se provodna folija nalazi. Sama antena se može sastojati od više slojeva, kako dielektrika tako i provodnika. Neke od primarnih karakteristika štampanih antena su mala cena, mogućnost masovne proizvodnje, lako formiranje antenskih nizova u više prostornih dimenzija. Sa antenskim nizovima moguće je postići veliki dobitak, i proizvoljnu širinu glavnog snopa zračenja.

Izbor materijala na kome će biti napravljena antena ima presudan uticaj na fundamentalne parametre antene: radni opseg, učestanost, dobitak, dimenzije. Veliki uticaj materijala je svakako na efikasnost antene, tj. gubitke. Gubici zavise od mnogih faktora, i menjaju se sa frekvencijom tako da je željena radna učestanost početni uslov za izbor odgovarajućeg materijala.

Gubici u mikrostripu mogu tipično biti podeljeni na: gubitke u dielektriku, gubitke u metalu, gubitke usled neželjenog zračenja i gubitke usled procesa izrade (tolerancija). Gubici usled neželjenog zračenja mogu biti izuzetno kompleksni, jer mogu poticati od više različitih izvora: parazitni modovi, površinski talasi, zračenje od strane napojne mreže, itd. Za antenu ovo može biti naročito problematično, jer pored smanjenja efikasnosti može prilično degradirati dijagram zračenja antene. Da bi se minimizovalo neželjeno zračenje opšti princip je korišćenje tankog dielektrika u odnosu na radnu učestanost i uskih vodova. U tankim dielektricima sa malim gubicima izraženim preko tanδ koji je definisan kao odnos imaginarnog i realnog dela kompleksne permitivnosti (1), gubici u metalu postaju dominantni.

$$\varepsilon_r = \varepsilon_r' - j\varepsilon_r'' = \varepsilon_r'(1-\tan\delta) \tag{1}$$

Na učestanostima oko 2.4 GHz i niže pretežno se koristi FR-4, zbog veoma niske cene i lake dostupnosti, na višim učestanostima koristi se znatno skuplji dielektrici poput Rogers 3000, 4000 ili 5000 serije. Na nižim učestanostima gubici u dielektriku su dominantni, pa se zbog toga gubici u dielektriku uzimaju kao primaran parametar za računanje gubitaka. Kod štampanih antena dielektrik pored toga što razdvaja provodne delove antene, se ponaša kao nosač provodnika. Na GSM opsegu se mogu koristi znatno deblje folije od tipičnih 17 mikrona. U ovom slučaju kao dielektrik se može koristiti vazduh, jer se debela folija neće deformisati pod svojom težinom. Vazduh ima dielektrične osobine slične vakuumu. Sa tanjom folijom kao dielektrične podloge moguće je koristi penaste materijale poput Rohacell-a koji imaju malu dielektričnu konstantu $\varepsilon_r \approx 1.05$ ($\tan\delta \approx 0.0002$).

Debljina folije koja će biti korišćena je određena na osnovu skin efekta, po kome će se struja sa rastom učestanosti koncentrisati u veoma tankom sloju po površini provodnika, [1]. Ovo je osnovni razlog zašto je moguće koristi veoma tanke folije kao provodnike na visokim učestanostima. Drugi veoma bitan razlog za korišćenje tankih folija na visokim učestanostima je površinska hrapavost folije, koja je ovde primaran uzrok gubitaka. Gubici u metalu tj. foliji postaju veoma izraženi i za dielektrik sa niskim tanδ postaju dominantni. Deblja folija će tipično imati veću hrapavost.

Dielektrična konstanta kao elementarna osobina dielektrika, primarno utiče na dimenzije antene. Za veći ε_r dimenzije antene će biti manje, ali takođe efekat površinskih talasa i neželjenog zračenja biće znatno više izražen. Vakuum ili vazduh bi za mnoge slučajeve bio idealan dielektrik. ε_r je disperzivan parametar. Za komercijalne dielektrike ε_r je tipično data kao prosečna numerička vrednost na 10 GHz, dobijena sa serije uzoraka korišćenjem određene metode, [2].

Kod mikrostripa linije električnog polja antene putuju između dva medijuma: dielektrika i vazduha. Za analizu se koristi koncept efektivnog dielektrika dielektrične konstante ε_{eff}. Po tome umesto nehomogene sredine uzima se da linije električnog polja prostiru kroz ekvivalentni homogeni dielektrik. ε_{eff} ima ogromni značaj, jer se može direktno odrediti merenjima, a relacija (2) između ε_{eff} i ε_r je dobro poznata, [1],

Nikola Bošković – Institut za fiziku, Univerzitet u Beogradu, Pregrevica 118, 11080 Zemun, Srbija (e-mail: nikolab@ipb.ac.rs).

Miloš Radovanović – Institut za fiziku, Univerzitet u Beogradu, Pregrevica 118, 11080 Zemun, Srbija (e-mail: rmilos@ipb.ac.rs).

$$\varepsilon_{\text{eff}} = \frac{\varepsilon_r + 1}{2} + \frac{\varepsilon_r - 1}{2} \frac{1}{\sqrt{1 + 12\frac{h}{w}}} \quad (2)$$

gde su h i w, debljina dielektrika i širina mikrostrip voda. Postoje još preciznije relacije koje uzimaju u obzir debljinu bakarne folije. Svaka relacije ima određenu grešku kao i uslove pod kojima je primenjiva. U ovom radu precizna korelacija između ε_{eff} i ε_r je određena na osnovu simulacionog modela.

Površinska hrapavost folije ne utiče samo na povećanje gubitaka u metalu sa rastom učestanosti, već takođe utiče na promenu faze prostiranja talasa, tj. utiče na promenu ε_{eff}, tako da na osnovu toga dva identična dielektrika sa različitim profilima bakarne folije mogu imati dosta drugačiju ε_{eff}, [3].

U ovom radu je prikazana širokopojasna analiza dielektrika Rogers 3003, debljine h = 0.127 mm, tanδ = 0.001, $\varepsilon_r \approx 3$.

II. Analiza i merenja

Jedan od najbitnijih faktora za dobijanje prototipa štampane antene koji se slaže sa proračunima i simulacijama je korišćenje tačnih parametara materijala. Ovo u praksi znači da korišćenjem parametara definisanih od strane proizvođača koji u većoj ili manjoj meri mogu odstupati od konkretnog primerka dielektrika, u startu unosi određenu grešku. Takođe različite metode za merenje dielektrične konstante neće nužno dati identične rezultate, [2]. Dobra praksa je da se pre izrade štampane antene izvrši procena dielektrične konstante na opsegu od interesa korišćenjem identičnog proizvodnog procesa kao za izradu same antene.

Za procenu dielektrične konstante u ovom radu korišćena je metoda faznih razlika, [4]. Ova metoda podrazumeva korišćenje vodova različitih dužina i poznatom razlikom u dužinama. Na osnovu merenja *S*-parametara oba voda, dobija se korelacija (3), između ε_{eff}, električne (ΔEL) i fizičke dužine (Δl) na posmatranoj frekvenciji f kao

$$\varepsilon_{\text{eff}} = \left(\frac{\Delta EL \cdot c}{360° \cdot f \cdot \Delta l} \right)^2 \quad (3)$$

gde je c brzina svetlosti u vakuumu. Fizičke dimenzije korišćenih vodova su: širina voda w = 0.2 mm, dužine vodova su 20 mm i 30 mm, tj. razlika je Δl = 10 mm. Za merenje je korišćen Anritsu VectorStar ME7838A VNA. Meren je opseg od 65-110 GHz, sa korakom od 10 MHz. Konektori su kalibrisani sa Triple-Offset-Short-Through (SSST) kalibracijom. Preciznost izrade vodova je oko 0.01 mm. Dimenzije vodova su merene pod mikroskopom.

Velika prednost ove metode je što se vrlo lako može dobiti širokopojasna karakteristika ε_r. Tačnost ove metode veoma zavisi od tačnosti izmerene razlike faza od datih vodova. Potrebno je koristi veoma kvalitetne širokopojasne konektore, bez lemljenja. Ovde su korišćeni Southwest Microwave 1 mm koaksijalni konektori za W-opseg, deklarisani za rad od 0 do 110 GHz.

Sl. 1. Balansni mikrostrip vod od bakarne folije na dilektriku.

U datom slučaju vršena su merenja i procena za dva različita slučaja bakarne folije. Za slučaj ED (elektro-deponovanog) bakra i za slučaj rolovane bakarne folije. Od interesa je utvrđivanje parametara za balansni mikrostrip [5], Sl. 1. Kao što se vidi za razliku od mikrostripa kod koga je jedan vod (masa) znatno širi od drugog voda, kod balansnog mikrostripa oba voda su iste širine. Ovo u praksi znači da će balansni vod biti delikatniji za fizičku obradu, jer oba voda moraju da se fizički obrade na odgovarajuće dimenzije.

Aparatura za merenje je prikazana na Sl. 2. Kako je dielektrik veoma tanak, napravljeni su metalni nosači koji drže dielektrik i konektore tokom merenja.

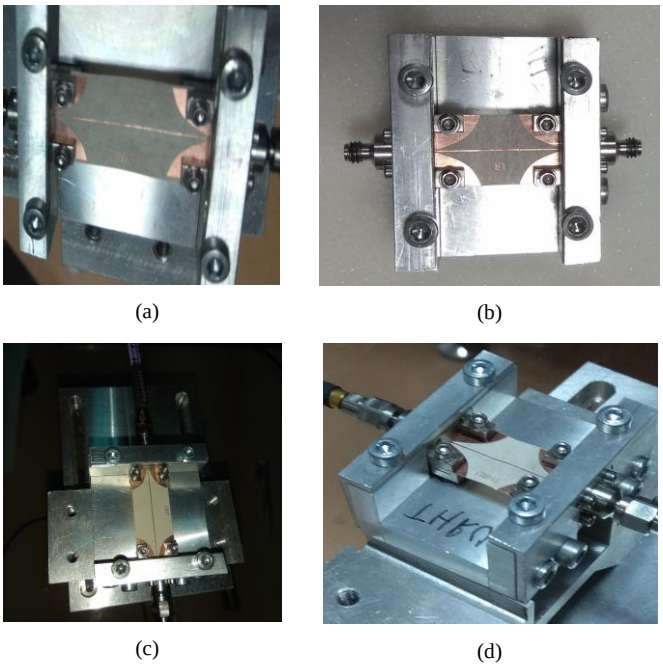

(a) (b) (c) (d)

Sl. 2. Vodovi različitih dužina na aparaturi za merenje *S*-parametara. Modeli sa rolovanom folijom (a-b) i ED folijom (c-d). Duži vodovi su dati pod (a) i (c).

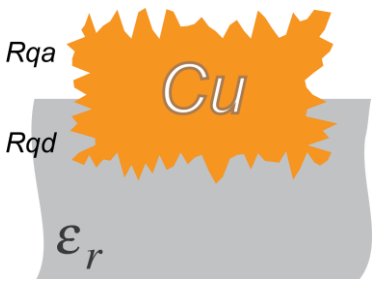

Sl. 3. Prikaz poprečnog preseka bakarnog voda uronjenog u dielektrik sa prikazanom hrapavosti između vazduha i folije (*Rqa*) i hrapavosti između folije i dielektrika (*Rqd*).

Hrapavost se tipično predstavlja preko srednjeg kvadratnog korena hrapavosti, *Rq* [6]. Za slučaj bakarne folije za dielektrike daju se dve, tipično različite vrednosti. Jedna za površinu okrenutu ka vazduhu (*Rqa*), a druga za površinu okrenutu ka dielektriku (*Rqd*), Sl. 3. *Rqd* će uglavnom imati značajno veću vrednost i za neke slučajeve se čak veštački uvećava kako bi se omogućila što čvršća veza između folije i dielektrika. U ovom slučaju za rolovanu foliju vrednosti *Rqd* i *Rqa* su 0.4 μm i 0.3 μm, dok za ED vrednosti su redom 2 μm i 0.4 μm. Simulirana širokopojasna karakteristika tanδ je dobijena na osnovu Debajevog modela višeg reda [7]. U korišćenom modelu uticaj tanδ je značajano manji u odnosu na uticaj gubitaka u metalu.

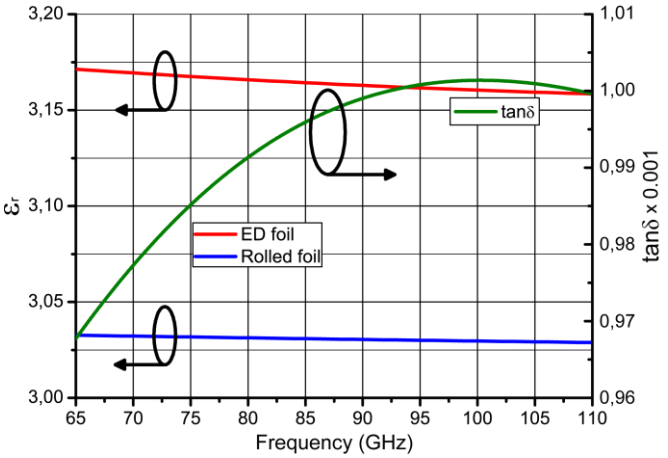

Sl. 4. Vrednosti ε_r dobijene na osnovu merenja i aproksimacija tanδ.

Sa Sl. 4 se vidi da na osnovu merenja ε_{eff} odgovarajuće vrednosti ε_r se značajno razlikuju, iako je u pitanju isti dielektrik. Takođe se vidi da za slučaj rolovane bakarne folije dielektrična konstanta je veoma slična deklarisanim vrednostima na 10 GHz, gde je uticaj hrapavosti daleko manji. Sa grubljim profilima bakarne folije razlika postaje značajna [3]. Kako su grublji profili daleko jeftiniji njihova upotreba je znatno veća. Samim tim je jasno da u većini slučajeva deklarisani parametri dielektrika neće dati realističan elektromagnetni model, već vrednosti dobijene na ovaj način treba da budu ulazni parametri odgovarajućeg modela.

Druga velika razlika će biti naravno u pogledu gubitaka. Totalni gubici po jedinici dužine se mogu dobiti takođe merenjem prototipa sa Sl. 2, iz vrednosti magnitude S_{12}. Za uračunanje gubitka u metalu često se koristi koncept efektivne provodnosti metala σ_{eff}, po kome se umesto 58 MS/m za provodnost bakra, uzima manja vrednost dok gubici u modelu ne postanu jednaki stvarnim gubicima. Ovaj model je odličan za brze proračune, međutim on je veoma uskopojasan. Postoji veliki broj znatno naprednijih modela, od kojih većina zahteva veliki broj parametara za kvalitetnu procenu.

Uporedo sa empirijskim razvijani su i simulacioni 3D modeli. Ono što je posebno problematično kod ovog pristupa je što zbog veoma malih dimenzija hrapavosti, čak i veoma mali modeli dimenzija 1 mm bi imali ogroman broj nepoznatih. Takođe i postavka samih modela se često zasniva na posmatranju površine kao fraktalne strukture. U praksi hrapavost je neuređena tj. svaki pik ili dolina imaće nešto drugačiju vrednost. Za primenu u polju mikrotalasne tehnike potreban je model, koji može na osnovu dostupnih parametra, da precizno proceni uticaj hrapavosti na prostiranje elektromagnetskih talasa.

Posebno zgodan je gradijentni model [8], po kome je moguće dobiti širokopojasnu procenu uticaja hrapavosti samo na osnovu *Rq*. Osnova ovog modela je da se umesto konstante vrednosti σ_{eff}, uzima vrednost dobijena na osnovu statističke kumulativne funkcije raspodele kao (4)

$$\sigma(x) = \sigma_{Cu} \int_{-\infty}^{x} \exp\left(-\frac{u^2}{2R_q^2}\right) du \qquad (4)$$

σ se posmatra kao funkcija rastojanja x u pravcu normalnom na površinu gde se nalazi bakarna folija. U ovom opsegu funkcija može imati sve moguće vrednosti od nule do provodnosti bakra bez hrapavosti σ_{Cu}.

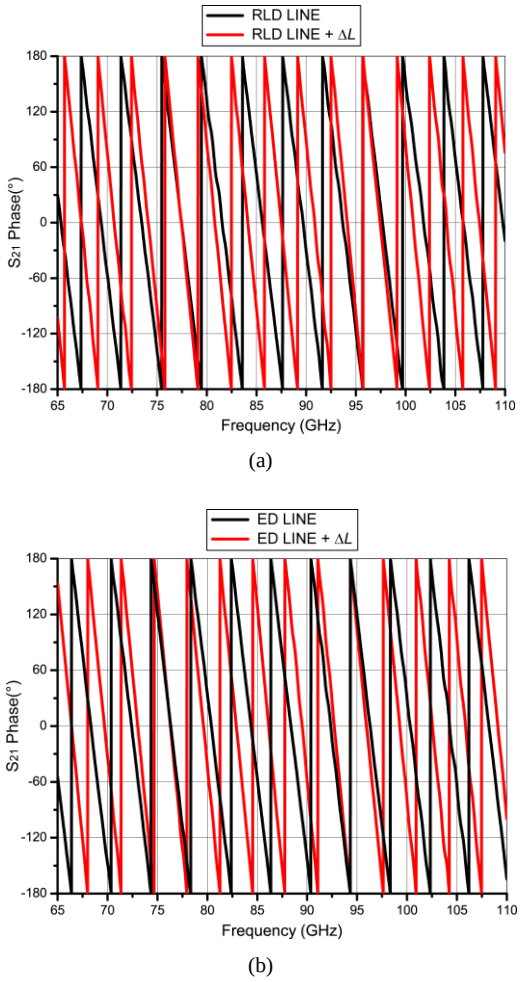

Sl. 5. (a) Merena faza kraćeg (crno) i dužeg voda (crveno) za slučaj rolovane bakarne folije, (b) merena faza kraćeg i dužeg voda za slučaj ED folije.

Merene fazne karakteristike vodova za različite tipove folija je data na Sl. 5, ΔL = 10 mm.

Procena doprinosa gubitaka od dielektrika je dobijena zamenom modela bakarne folije sa idealnim električnim

provodnikom $\sigma = \infty$, Sl. 6. Dok se uticaj gubitaka u metalu može dobiti uzimanjem da je tanδ = 0. Po ovome modelu sa Sl. 6 se vidi da je uticaj gubitaka u dielektriku daleko manji nego u metalu. Vidi se da gradijentni model može dosta dobro da isprati promenu gubitaka sa frekvencijom. Očekivano, gubici su znatno veći za ED bakarnu foliju.

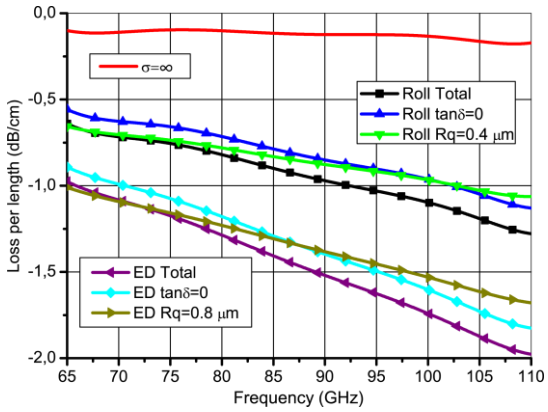

Sl. 6. Mereni totalni gubici za slučaj sa rolovano bakarnom folijom (Roll Total) i ED folijom (ED total), procena uticaja gubitaka u metalu i dielektriku za date folije, i poređenje sa odgovarajućim gradijentnim modelom.

III. Zaključak

U radu je prikazan je značaj merenja parametara materijala pre izrade samog prototipa antene. Deklarisani parametri materijala na 10 GHz nisu pouzdani za više učestanosti, naročito u pogledu promena karakteristika samog materijala na velikom opsegu učestanosti. Za tačan model potrebno je proceniti parametre materijala preko merenja u opsegu od interesa.

Zahvalnica

Autori se zahvaljuju Ministarstvu prosvete, nauke i tehnološkog razvoja Republike Srbije za finansiranje istraživanja.

Literatura

[1] D. M. Pozar, "*Microwave Engineering*", 4th ed., Wiley, 2011.
[2] J. Coonrod and A. F. Horn III, "Understanding Dielectric Constant for Microwave PCB Materials," *High Frequency Electronics*, July 2011.
[3] A. F. Horn III *et al*., "Effect of conductor profile on the insertion loss, phase constant, and dispersion in thin high frequency transmission lines", *DesignCon 2010*, Santa Clara, February 2010.
[4] N. K. Das, S. M. Voda and D. M. Pozar, "Two Methods for the Measurement of Substrate Dielectric Constant," in *IEEE Trans. Microw. Theory Techn.*, vol. 35, no. 7, pp. 636-642, Jul 1987.
[5] N. Boskovic *et al*., "Printed Frequency Scanning Antenna Arrays With Enhanced Frequency Sensitivity and Sidelobe Suppression," *IEEE Trans. Antennas Propag*., vol. 65, no. 4, pp. 1757-1764, April 2017.
[6] Rogers Corporation, "Copper Foils for High Frequency Materials", *Data Sheet*, 2015.
[7] F. Maradei, H. Ke and T. H. Hubing, "Full-Wave Model of Frequency-Dispersive Media With Debye Dispersion Relation by Circuit-Oriented FEM," *IEEE Transactions on Electromagnetic Compatibility*, vol. 51, no. 2, pp. 312-319, May 2009.
[8] G. Gold and K. Helmreich, "A physical model for skin effect in rough surfaces," *2012 42nd European Microwave Conference*, Amsterdam, 2012, pp. 1011-1014.

Abstract

Choice of the material play crucial role in the printed antenna design. This is especially critical on the W-band, where the loss mechanism is significantly enhanced, which is why a very small number of standard dielectrics can be used. To suppress parasite modes and surface waves, dielectric thickness must be very small relative to the frequency. Here, the effect of surface roughness of the copper conductor foil has a dominant impact on losses. This paper presents the importance of choosing an appropriate foil and following consequences. The conclusions are accompanied by simulations and measurements.

Material Characteristics for Printed Antenna Applications at 65-110 GHz

Nikola Boskovic and Milos Radovanovic

Influence of Various EM Models of an Aircraft to Monostatic RCS

Tomislav Milošević

***Abstract*—This paper outlines influence of four EM models of an electrically large aircraft on monostatic RCS results at 2.00 GHz. The differences in calculated RCS results suggest the importance of a choice of an EM model depending on the particular scope. The paper provides better understanding of some of EM scattering effects frequently addressed by engineering, scientific and military working groups interested in RCS. Software tool used for simulations and model manipulations is a full wave 3D EM Method-of-Moments based software with Surface Integral Equations applied to quadrilateral mesh elements.**

***Index Terms*—Scattering, aircraft, RCS, simulation.**

I. Introduction

CALCULATION of scattering from electrically large aircrafts is often a subject of interest of scientific, engineering, or military working groups. The purpose of scattering calculation can vary from an academic discussion, to simulation software testing, to anti-aircraft defense tactics preparation. Sometimes a calculation of scattering from electrically large fighter aircrafts is driven by marketing as various teams simulate fighter aircrafts in order to impress existing or future customers. According to information coming from various open sources, pure metallic models of aircrafts are still fashionable in various electromagnetic (EM) software tools (for example, the models of 4th generation of fighter jets are still widely used). They are usually modeled as metallic surfaces. Regarding the shape of an aircraft model, the details are usually classified and the shape usually comes rather from loose visual impression then from precise engineering data. For the sake of modeling some details are usually simplified, e.g., the engine intake is terminated with a metallic plate. The problem of inaccurate modeling arises when such model is chosen as the reference model in a realistic scenario.

The scattering results are usually related with radar operations and obtained after illuminating a target (an aircraft) with a plane wave. This paper will consider monostatic scattering and illumination with EM wave containing electric field with the E_θ component, only [1].

In monostatic radar setup the same antenna is used for both transmitting and receiving the signal. Complex radar targets such as aircrafts generally have (monostatic) cross sections that vary rapidly with frequency and aspect angle. Actually, a radar target is characterized by its radar cross section, which gives the ratio of scattered power to incident power density. The ratio depends on the target shape, the frequency and the polarization of the incident EM wave, and on the incident angle relative to the target. Monostatic radar cross section (RCS) can be defined as RCS where angles of incident and reflected waves are identical. In general, more complex targets require more efficient numerical techniques for software simulations [2].

Here, we will consider four EM models of a single representative sample in the form of the 4th generation fighter aircraft. The EM models encompass scenarios where:

- The aircraft canopy and the radome are modeled as metallic surfaces while the engine intake is terminated with a metallic plate.
- The aircraft canopy and the radome are modeled as metallic surfaces while the engine intake can be considered as one-side open cavity with a metallic plate located in front of the jet engine rotor blades.
- The aircraft canopy is modeled as a metallic surface, the radome is excluded exposing a flat surface of the radar antenna while the engine intake is in the form of the open cavity.
- The aircraft canopy is excluded from the model exposing a pilot's working area which is also an open cavity. The radome is excluded exposing a flat surface of the radar antenna. The engine intake is in the form of the open cavity.

The results of monostatic RCS simulations of the four models will be compared and discussed. The aircraft dimensions and shape are to some degree approximate with the respect to actual aircraft.

The simulations will be facilitated in the frequency domain. In this paper, WIPL-D Software, a full wave, 3D EM frequency-domain Method-of-Moments (MoM) based software will be exploited for importing and modifying available CAD file and simulations applying higher order basis functions on quadrilateral mesh elements with Surface Integral Equations [3]. Since radar frequencies used for long range surveillance are located within L-band between 1 GHz and 2 GHz [4] and airport surveillance primary radar frequencies are about 2.8 GHz [5], the models presented here will be simulated in-between these frequencies trying to grasp EM effects appearing at both bands. Thus, the EM models of the aircraft are simulated at frequency of 2 GHz.

II. Aircraft EM Models

Four CAD models of the aircraft are shown in Figs. 1-4. All models are displayed with a symmetry plane. The symmetry plane represents a software feature where a symmetry of the structure is exploited to reduce an original number of unknowns. The original number of unknowns is approximately halved. Each figure also contains a magnified detail of an aircraft model. For all models it is assumed that aircraft surfaces are perfect electrically conductive metal. The models were imported and subsequently modified to

Tomislav Milošević is with WIPL-D d.o.o., Gandijeva 7, 11073 Belgrade, Serbia (e-mail: tomislav.milosevic@wipl-d.com).

have lower surfaces of wings smooth i.e., without pylons intended for carrying various loads.

The first model, which is shown in the Fig. 1 represents the model with the aircraft canopy and the radome modeled with metallic surfaces, while the engine intake is terminated with a metallic plate. This model is probably the most often seen in various software presentations and booklets. Fig. 1 also contains approximate dimension of the model which can be referenced when estimating the dimensions of the other models. In general, the model shown in the Fig. 1 is suitable for simulations with geometrical\physical optic-based EM solvers since the cavity in the form of engine intake is practically excluded from the simulation. From the marketing point of view this model mimics very well the realistic aircraft structure.

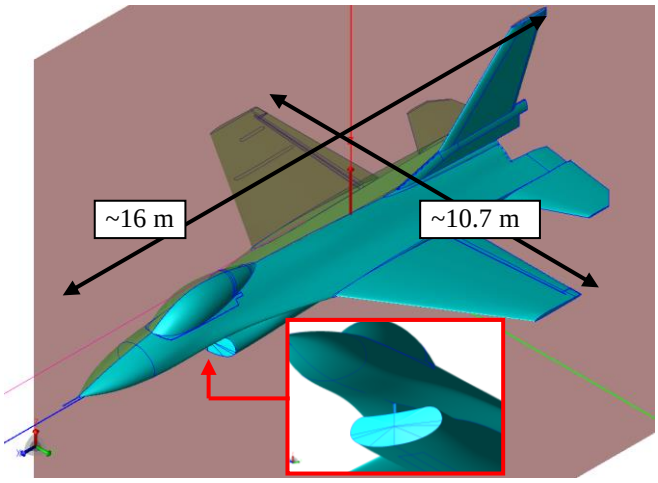

Fig. 1. The aircraft canopy and the radome are modeled as metallic surfaces while the engine intake is terminated with a metallic plate. This is probably the most commonly used EM model of an aircraft.

The second EM model shown in the Fig. 2 represents the model where the aircraft canopy and the radome are modeled as metallic surfaces while the engine intake can be considered as an open cavity with a metallic plate located in front of the jet engine rotor blades. Such model can also be often seen in various software presentations and booklets, despite presence of the cavity.

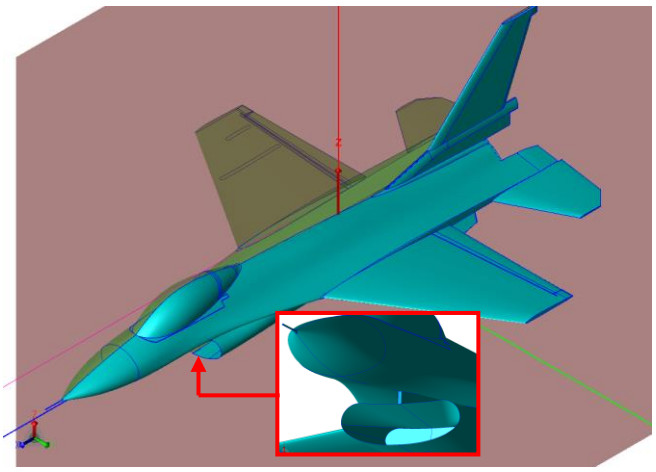

Fig. 2. The model of the aircraft which is also often simulated. The aircraft canopy and the radome are modeled as metallic surfaces while the engine intake can be considered as an open cavity with a metallic plate located in front of the jet engine rotor blades.

The third model is shown in the Fig. 3 and it can be used as a good representation for many types of aircrafts. In order to reduce influence of the pilot working area to RCS which also represents a sort of an open cavity (see also Fig. 4), some aircraft real-life models have canopy painted with the special material which is visually transparent and which increases radar waves reflection [6]. This model has the aircraft canopy modeled as a metallic surface, while the airborne radome covering radar antenna and providing aerodynamic streamlining is excluded from the model exposing radar antenna flat surface. Removing radome is justified as the radomes are generally composed of low-loss dielectrics materials [7]. The assumption applied here is that the radome is transparent for EM waves with frequency of 2 GHz. The engine intake is again in the form of an open cavity.

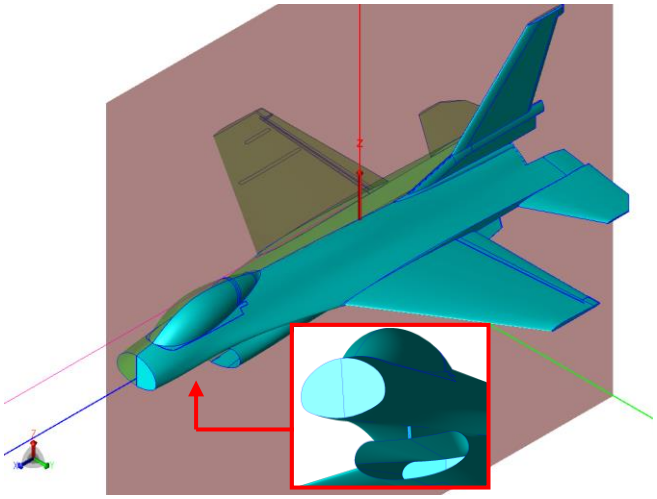

Fig. 3. The model of the aircraft where the aircraft canopy is modeled as a metallic surface, the radome is excluded exposing radar antenna flat surface while the engine intake can be considered as an open cavity with a metallic plate located in front of jet engine rotor blades.

Finally, the fourth EM model is shown in the Fig. 4.

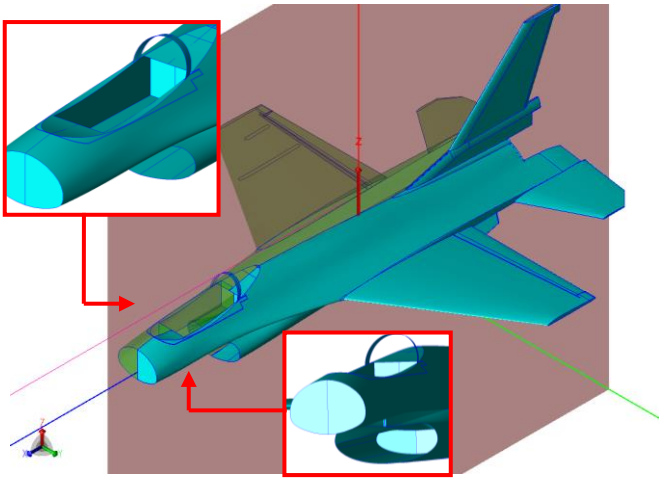

Fig. 4. The model of the aircraft which is probably the most rarely seen. The aircraft canopy is excluded from the model exposing an open cavity which represents a pilot's working space. The radome is excluded exposing radar antenna flat surface. The engine intake is in the form of an open cavity with a metallic plate located in front of jet engine rotor blades.

The model shown in the Fig. 4 encompasses the aircraft canopy excluded from the model exposing cavity representing a pilot's working area. The assumption applied here is that the canopy is transparent for EM waves with frequency of 2 GHz. Also, the radome is excluded exposing radar antenna flat surface. The engine intake is in the form of an open cavity.

In order to define suitable nomenclature of the models, four acronyms will be introduced. The model shown in the Fig. 1 will be named and referred further as MMM since the radome, the canopy, and the termination of the cavity are modeled with metallic surfaces (metal-metal-metal, respectively).

The model shown in the Fig. 2 will be named and referred further as MMA since the radome, and the canopy are modeled with metallic surfaces, while the termination of the cavity is excluded (it is assumed that it is modeled with air surface). In that sense, the name of the model will be MMA (metal-metal-air, respectively).

The model shown in the Fig. 3 will be named and referred further as AMA since the radome is replaced with air, the canopy is modeled with metallic surfaces while the termination of the cavity is excluded (again, it is assumed that it is modeled with air surface). In that sense, the name of the model will be AMA (air-metal-air, respectively).

The model shown in the Fig. 4 will be named and referred further as AAA since the radome, the aircraft canopy, and the termination of the cavity are all excluded from the model (assuming that all of them they are modeled with air surfaces). In that sense, the name of the model will be AAA (air-air-air, respectively).

Meshing details of the four models are presented in the Fig. 5-Fig. 8.

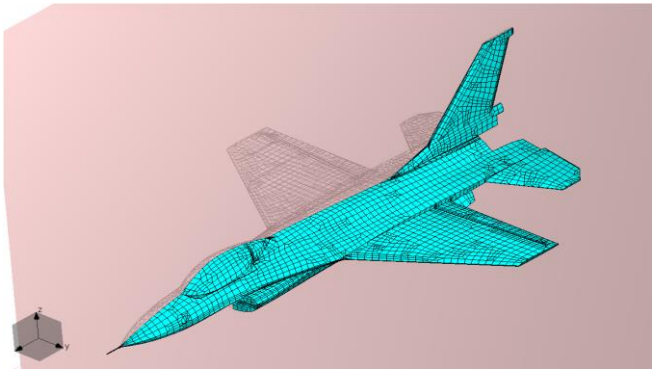

Fig. 5. Meshed metal-metal-metal (MMM) model

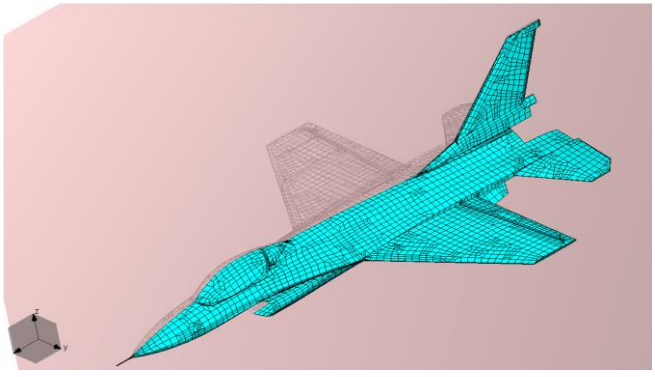

Fig. 6. Meshed metal-metal-air (MMA) model.

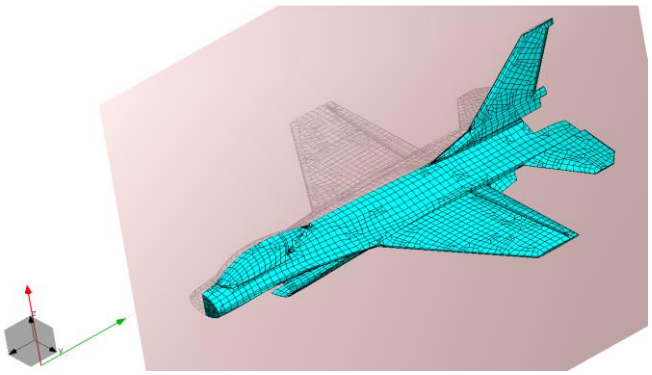

Fig. 7. Meshed air-metal-air (AMA) model.

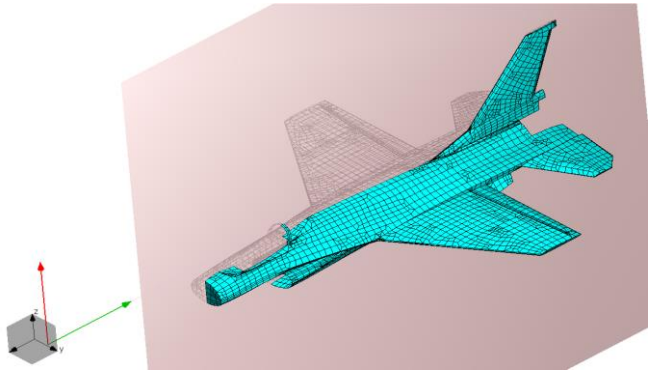

Fig. 8. Meshed air-air-air (AAA) model.

These four figures (Fig. 5-Fig. 8) depict meshed EM models i.e., models after applying mesh procedure and converting CAD files to simulation software native format. In the software native format, the aircrafts are modeled by using bilinear quadrilateral surfaces

III. Simulation Results

In order to discuss the influence of various aircraft modelling approaches, the calculated monostatic scattering results for four EM models follow. For the reasons of the careful comparison, it is convenient to present in the same graph the results originating from a pair of two models (three pairs in total, MMM-MMA, MMA-AMA and AMA-AAA). Eventually, MMM and AAA models will be compared.

All the results are obtained after calculating monostatic scattering from the front area of the aircraft. Actually, monostatic scattering is calculated in 901 directions encompassing theta angle span from 45 degrees below to 45 degrees above the aircraft nose. It is adopted that angle $\theta = 0$ degrees points toward aircraft nose (actually, it points toward horizon). The orientation of the aircraft and the theta angle are shown in Fig. 9.

All of the models have been simulated at operating frequency of 2 GHz. The workstation used for the simulations is Intel® Xeon® Gold 5118 CPU @ 2.30GHz 2.30 GHz (2 processors) with 192 GB RAM and 4 GPU cards Nvidia GeForce GTX 1080 Ti used for matrix inversion.

The most time-consuming simulation is MMA requiring less than 90 minutes to complete the simulation. Also, it requires 224,852 unknowns. The model MMM requires 218,601 unknowns while the model AMA requires 192,756 unknowns. Finally, the model AAA requires 193,419 unknowns.

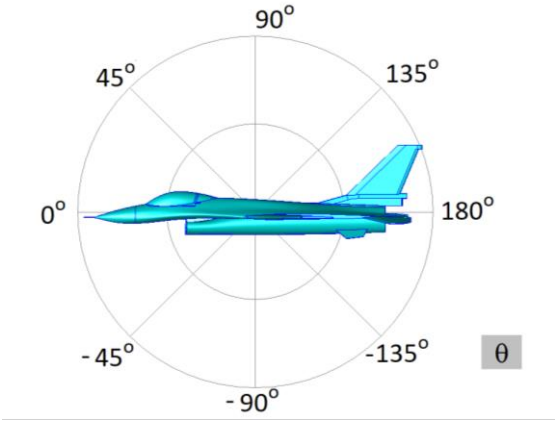

Fig. 9. Theta angle and the orientation of the aircraft.

A. *Comparing Results: MMM vs. MMA*

The comparison between MMM and MMA results is shown in the Fig. 10. A strong influence of cavity presence can be seen there. Actually, completely different results are obtained for angles between approximately -45 degrees and 5 degrees where, on average, the results differ by approximately 15 dB. This angle span corresponds to the angles of incidence important for ground-based surveillance radars.

The monostatic RCS for angles higher than about 10 degrees is almost the same for both models. It is expected since these directions are not affected by a way of terminating the engine intake, in this case located below the aircraft.

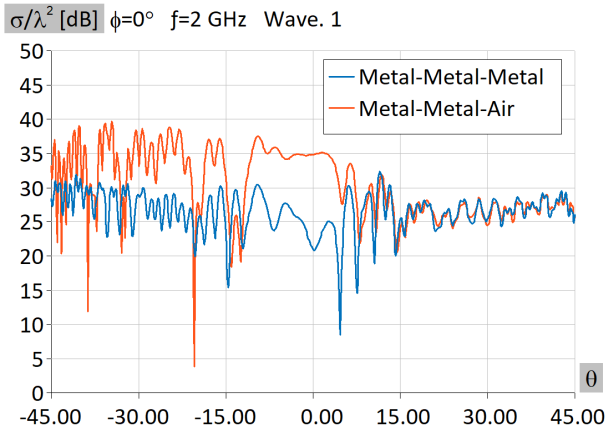

Fig. 10. Monostatic normalized RCS: MMM vs. MMA

B. *Comparing Results: MMA vs. AMA*

The comparison between MMA and AMA results is shown in Fig. 11. The only difference appears around 0 degrees. This is expected since the main difference between these two EM models appears in the area of the aircraft nose. This difference is significant in environment scenarios in which the aircraft is illuminated from the horizon (e.g., if an aircraft nose is illuminated from another airborne surveillance radar).

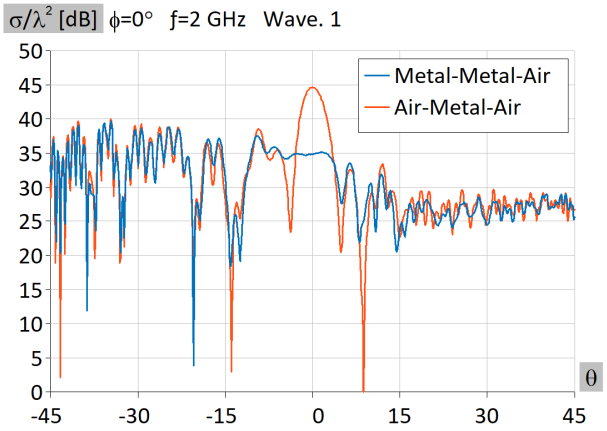

Fig. 11. Monostatic normalized RCS: MMA vs. AMA.

C. *Comparing Results: AMA vs. AAA*

The comparison between AMA and AAA results is shown in the Fig. 12. The influence of representing pilot's working area as an open cavity is clearly seen in the scattering directions above theta angle of about 15 degrees. The reason for the differences can be explained similarly as in the MMM-MMA case - the presence of the cavity increases monostatic normalized RCS level.

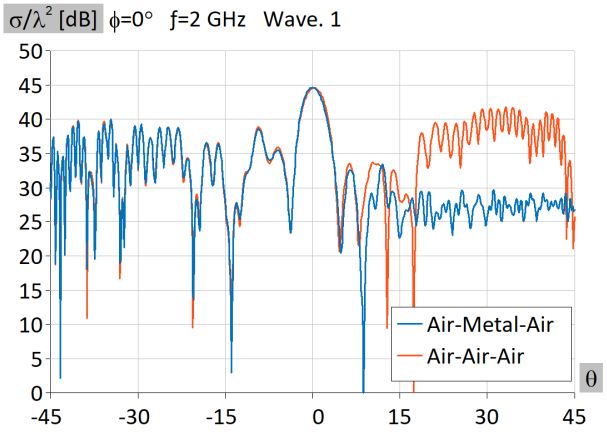

Fig. 12. Monostatic normalized RCS: AMA vs. AAA.

D. *Comparing Results: MMM vs. AAA*

In order to compare the two extreme cases considered in this paper, (MMM-AAA), calculated monostatic normalized RCS results are presented in the Fig. 13. The differences are considerable in the whole range of theta angles (-45 deg, 45 deg), but the origin for the differences can be easily tracked and explained in each of three mentioned subranges due to the previous three analysis and comparisons.

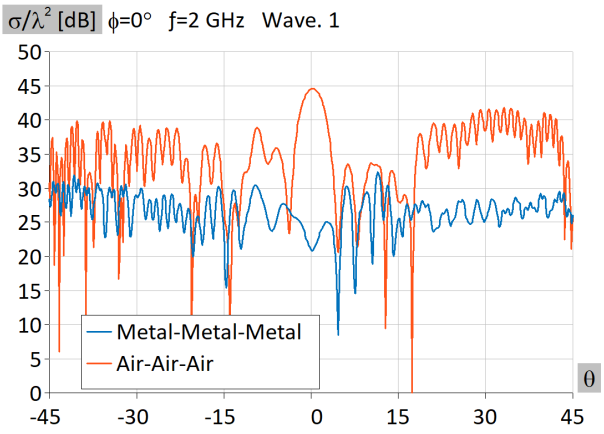

Fig. 13. Monostatic normalized RCS: MMM vs. AAA.

IV. Conclusion

This paper outlines influence of various EM models of an aircraft to monostatic normalized RCS results. The software tool used for the simulations and the model manipulations was a full wave 3D EM Method-of-Moments based software with Surface Integral Equations applied to quadrilateral mesh elements.

The simulated fighter aircraft is modeled using PEC metallic surfaces. The operating frequency is selected to be between frequencies of acquisition radar and frequencies of airport surveillance primary radar. The excitation is a linearly polarized EM plane wave containing only theta component of the electric field.

Four simulated EM models of the aircraft represent four common cases of aircraft models. Starting from a widely accepted model of the aircraft, named MMM here, the models are modified by adding or removing metallic surfaces, while dielectric properties of the surfaces are ignored.

A relevant EM model of the aircraft is related to a particular purpose, from the software marketing to the various military scenarios. From the marketing point of view, the adequate model contains the least modifications and it is easily understandable (MMM). However, for modeling real-life aircraft and obtaining results required for military purposes, the models similar to AMA or AAA should be used. The two models exhibit significant EM effects coming from the details such as jet engine intake, radome and aircraft canopy and are not expected at the first glance.

This aircraft represents to some extent a large and complex radar target. Thus, it can be assumed that in a specific angle span, monostatic RCS levels change if some parts of the aircraft are replaced with another parts. This assumption can be identified easily in the Fig. 11, where a flat plate produces significantly larger reflection compared to a conical shape representing metallic aircraft nose. An effect of this kind is expected, due to the nature of an EM wave scattering from the metallic surfaces of various shape. The similar effect can be noticed if a drop shaped canopy (or flat plate terminating the engine intake) is replaced with the open cavity. Since the aircraft is large and the reflections from these areas are assumed to be almost independent, all the effects presented in Fig. 13 using a single aircraft model can be also obtained by concatenating separately obtained results shown in Figs. 10-12.

The high efficiency of computation can be confirmed through the simulation times as they are all relatively short considering electrical size of the simulated structure and the workstation used.

The further investigation of this structure will include influence of the gun pipe and presence of various door openings to monostatic scattering. Also, further investigation will include application of radar-absorbing materials to selected aircraft surfaces in order to decrease a scattering level.

References

[1] B. M. Kolundzija, A. R. Djordjevic, *Electromagnetic Modeling of Composite Metallic and Dielectric Structures, 1st* ed. Norwood, Massachusetts, USA: Artech House, 2002.

[2] D. M. Pozar, *Microwave Engineering, 2nd* ed., USA, John Wiley & Sons, 1998.

[3] WIPL-D Software, WIPL-D d.o.o, Belgrade 2021. www.wipl-d.com

[4] https://www.radartutorial.eu/07.waves/Waves%20and%20Frequency%20Ranges.en.html

[5] https://en.wikipedia.org/wiki/Airport_surveillance_radar

[6] https://en.wikipedia.org/wiki/Aircraft_canopy

[7] J. L. Volakis, *Antenna Engineering Handbook, 4th* ed., USA: McGraw-Hill, 2007.

Utilization of Characteristic Mode Analysis in Coupled Resonators Microstrip Filter Design

Ana Đurđević and Milka Potrebić, *Member, IEEE*

***Abstract*—Examination of resonant frequency and coupling coefficient is essential part in microwave filters design with coupled resonators. We introduce Characteristic Mode Analysis (CMA) based method for calculation of coupling curve, applied to microstrip resonators. The main advantage of this approach is simplicity, due to CMs independency of any external sources. The results for coupling curve are presented and cross-checked with results obtained by equivalent two ports microstrip model with feeding lines. A very good agreement between the two methods is observed.**

***Index Terms*—Coupling coefficient, coupled resonators, CMA, filter, resonant frequency.**

I. Introduction

DISHAL acknowledged that any narrow-band bandpass filter can be described by tuning frequency of the resonators, the couplings between adjacent resonators and the external *Q*-factor of the first and last resonators [1], [2]. Initially, in case of distributed resonators, these parameters had usually been determined without a straight-forward method, but rather with a set of numerous experiments and measurements. With expansion of electromagnetic (EM) solvers, generating design curves for coupling and external *Q*-factor in terms of variables of interest became significantly easier. In [3], it was demonstrated how to extract the curves from insertion loss response and time delay at resonances, obtained from EM simulations. That approach we will later use in order to verify our results.

Since it was introduced, Characteristic Mode Analysis (CMA) was mainly used to analyze radiating properties of various antennas and scattering objects [4]–[6]. Apart from these fields, it found a role in analysis of surface wave resonance as well [7]. In this paper we outline a method for investigating resonant frequencies and generating coupling curve between resonators using CMA theory, in example of microstrip coupled resonators. We haven't yet considered a way to determine external *Q*-factor using CMA, which would allow to apply Dishal's concept [2] with all three variables required for bandpass filter design obtained by CMA only. The main purpose of this paper is to indicate a potential of CMA as a tool in narrow-band microwave bandpass filter design.

Chosen example for presenting the method consists of two grounded $\lambda/4$ resonators in microstrip technique, designed on operating frequency 1 GHz. To take advantage of Characteristic Modes formulation for PEC bodies [8], we considered air substrate. All the full-wave 3D EM analysis was performed in WIPL-D software package [9], which utilizes MoM (*Method of Moments*) and HOBFs (*Higher Order Basis Functions*).

II. Theoretical Insight to Characteristic Modes Analysis

Characteristic mode analysis is the numerical calculation of a weighted set of orthogonal current modes that are supported on a given structure. The theory was first introduced to electromagnetic by Garbacz [3], and later Harrington and Mautz formulated generalized eigenvalue equation for conducting bodies applied on MoM impedance matrix [8]. Here follows brief insight to derivation of eigenvalue equation. When an incident plane wave $\mathbf{E}^{\mathrm{i}}$ illuminates PEC structure, it induces surface currents $\mathbf{J}_{\mathrm{s}}$, which induce scattered field $\mathbf{E}^{\mathrm{s}}$. Boundary condition for $\mathbf{E}$ filed on the PEC body surface S can be written as:

$$(\mathbf{E}^{\mathrm{i}}(\mathbf{r})+\mathbf{E}^{\mathrm{s}}(\mathbf{r}))_{\tan}=0,\ \ \mathbf{r}\in S, \tag{1}$$

where "tan" denotes tangential components of electric field. Scattering field $\mathbf{E}^{\mathrm{s}}$ can be expressed in terms of induced surface current as:

$$\begin{aligned}\mathbf{E}^{\mathrm{s}} &= -\frac{j\omega\mu_0}{4\pi}\int_S G(\mathbf{r},\mathbf{r}')\mathbf{J}_s(\mathbf{r}')dS' \\ &\quad -\frac{j}{4\pi\varepsilon_0\omega}\nabla\int_S G(\mathbf{r},\mathbf{r}')\nabla'\mathbf{J}_s(\mathbf{r}')dS'\end{aligned} \tag{2}$$

where ε_0 and μ_0 are the permittivity and permeability of the free space, and $G(\mathbf{r},\mathbf{r}')$ is Green's function in free space multiplied by 4π, and given by

$$G(\mathbf{r},\mathbf{r}')=\frac{e^{-jk_0R}}{R},\ \ R=|\mathbf{R}|,\ \ \mathbf{R}=\mathbf{r}-\mathbf{r}', \tag{3}$$

where R is distance between the field and the source point and $k_0=\sqrt{\varepsilon_0\mu_0}$ is the wavenumber in free space. Relationship

Ana Djurdjevic is with WIPL-D d.o.o., Gandijeva 7, apt. 32, 11073 Belgrade, Serbia, and she is also a master student at the School of Electrical Engineering, University of Belgrade, Bulevar kralja Aleksandra 73, 11020 Belgrade, Serbia (E-mail: ana.djurdjevic@wipl-d.com).

Milka Potrebic is with the School of Electrical Engineering, University of Belgrade, Bulevar kralja Aleksandra 73, 11020 Belgrade, Serbia (E-mail: milka_potrebic@etf.rs).

between scattering field and surface currents can be written in form of integro-differential operator $L(\cdot)$, thus boundary condition (1) can be expressed as:

$$\left[L(\mathbf{J}_s)\right]_{\tan} = \mathbf{E}^{\mathrm{i}}_{\tan}(\mathbf{r}),\ \mathbf{r} \in S \tag{4}$$

that is known as EFIE (*Electric Field Integral Equation*). If we write tangential component of $L(\cdot)$ operator as a new operator $Z(\cdot)$, we obtain:

$$\left[L(\mathbf{J}_s)\right]_{\tan} = Z(\mathbf{J}_s). \tag{5}$$

Operator $Z(\cdot)$ has impedance property and can be split into real and imaginary part as:

$$\mathbf{Z} = \mathbf{R} + j\mathbf{X} \tag{6}$$

which represents MoM impedance matrix. By using impedance matrix in weighted eigenvalue equation, generalized eigenvalue equation for CM calculation is defined as:

$$\mathbf{X}(\mathbf{J}_{s,n}) = \lambda_n \mathbf{R}(\mathbf{J}_{s,n}). \tag{7}$$

Solutions of (7) are eigenvectors $\mathbf{J}_{s,n}$, that are vectors of current coefficients, eigenvalues λ_n, and n is the order of each mode. Eigenvalue is the real number within a range $[-\infty, +\infty]$, and its magnitude is proportional to the total stored field energy:

$$\omega \iiint_V (\mu \mathbf{H}_n \cdot \mathbf{H}_n^* - \varepsilon \mathbf{E}_n \cdot \mathbf{E}_n^*) \mathrm{d}V = \lambda_n. \tag{8}$$

Physical meaning of eigenvalues can be interpreted as follows:

- In the case of $\lambda_n = 0$, stored electric and magnetic energies are equal, and associated modes are considered as the resonant modes.
- In the case of $\lambda_n < 0$, stored electric energy dominates, and associated modes are considered as the capacitive modes.
- In the case of $\lambda_n > 0$, stored magnetic energy dominates, and associated modes are considered as the inductive modes.

The more convenient way for graphical representing eigenvalue is parameter called Modal Significance, defined as:

$$\mathrm{MS} = \left| \frac{1}{1 + j\lambda_n} \right| \tag{9}$$

MS takes values from [0,1], and for resonant modes, when λ_n approaches to 0, it is close to 1.

The important property which can be noticed from (7), is that CMs do not depend on any external excitation, but on the physical properties of the structure only. MoM matrix is filled-in, after which eigenvalue equation is solved in order to calculate unknown current coefficients for each mode, i.e. eigenvectors, as well as eigenvalues. Consequently, there is no need for any feeding network in analysis of the resonant properties in this way.

As it is mentioned before, the reason for analysis of PEC body in free space is to present the research using available tool [9]. In [10], theory of characteristic modes for material bodies is introduced, where the main difference from the theory for perfectly conducting bodies lies in the computation of the modes. It is also discussed in [10] that characteristic modes in material bodies have the most properties as corresponding modes in perfectly conducting bodies. Having that in mind, we may assume that the method is also valid for microstrip with other dielectric properties.

III. Generating Coupling Curve

Generally speaking, coupling coefficient can be defined as a ratio of coupled energy to stored energy, while corresponding electric and magnetic fields should be calculated at resonant frequencies [11]. In [12] it is given the expression for coupling coefficient, derived from lumped-element circuits:

$$k = \left(f_2^2 - f_1^2\right) \Big/ \left(f_1^2 + f_2^2\right), \tag{10}$$

where f_1 and f_2 are the lower and upper resonant frequency of the coupled resonators. Equation (10) is also valid for the distributed resonators, and resonant frequencies can be determined from full wave EM simulations. In following examples, coupling coefficient is always calculated using (10), while required resonant frequencies are obtained from both CMA and insertion loss response from model with feeding lines and ports. As an electromagnetic coupling increases when the elements are getting closer to each other, it is significant to graphically represent it as a function of distance, thus to generate coupling curve.

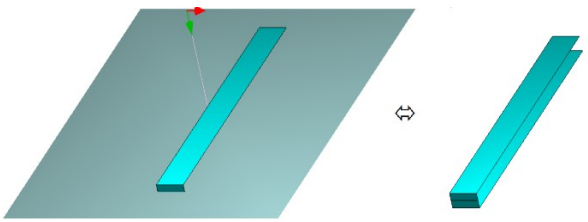

Fig. 1. Single grounded resonator above infinite PEC plane.

A. CMA Based Method and Numerical Model

Firstly, a single λ/4 resonator at operating frequency 1 GHz, with a grounded end above PEC plane, is analyzed with CMA solver. Distance from PEC plane is $h = 2$ mm, length of resonator $l = 74.95$ mm, and width $w = 9.83$ mm. In CMA

model it is not possible to define a port between ground and resonators that would introduce a voltage necessary for transmission line. This obstacle is overcome by defining an infinite PEC plane that indicates the image theory to be applied. The original and the equivalent model after image theory are applied as given in Fig. 1.

Analysis is performed in discrete frequency points, in range from 0.8 GHz to 5 GHz. MS for the first 3 modes is shown in Fig. 2.

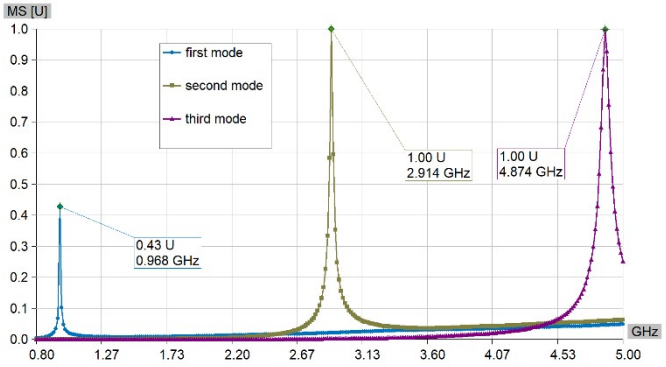

Fig. 2. MS for the first three modes of single resonator in frequency range 0.8 GHz – 5 GHz.

It can be seen from Fig. 2, that in the analyzed range there are three very narrow resonant modes, and the one of interest is at around 0.968 GHz. In order to analyze the coupling, one more resonator is added with the same dimensions, but grounded on different end, as shown in Fig. 3, and the results are given on Fig. 4. This model of coupled resonators is important for interdigital bandpass filter design.

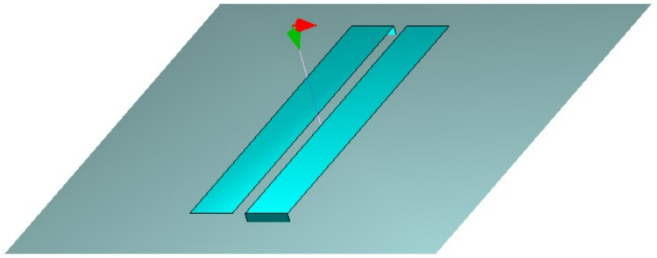

Fig. 3. Two coupled grounded resonators above infinite PEC plane.

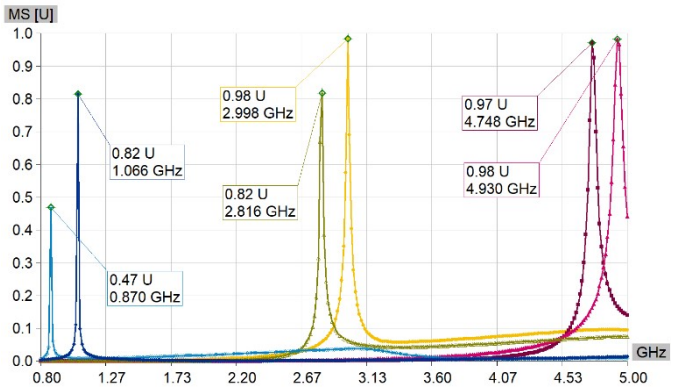

Fig. 4. MS for the first six modes of two coupled resonators in frequency range 0.8 GHz – 5 GHz.

As it was expected, instead of each resonance in case of single resonator, now we have two resonances shifted in frequency. Each peak still comes from different characteristic mode, but the two in every pair is very physically similar to each other, meaning have similar current and near field distribution. With varying the spacing between resonators, the spikes appear in the different positions in frequency. Having the low and high resonant frequencies as the only unknown quantities in (10), coupling coefficient can be calculated easily. In this example for spacing $s = 1$ mm, coupling coefficient equals to 0.2.

B. Method Based on Insertion Loss Response

In order to cross-check calculated results for coupling obtained by CMA method, we created the equivalent microstrip model with two resonators and two loosely coupled feed lines, presented in Fig. 5. The dielectric is air. The distances between feed lines and resonators equals to $2h$. Two resonators are grounded and two ports are placed on the different ends of feeding lines. The length and the width of the ground plane equal to 135 mm and 100 mm, respectively. The insertion loss response ($IL = -20\log_{10}|s_{21}|\,\mathrm{dB}$) is given in Fig. 6, and it can be observed that six resonances appeared at the same frequencies as resonances shown in MS response in Fig. 4.

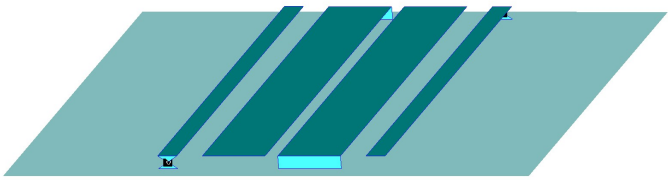

Fig. 5. Equivalent model with resonators and feeding lines.

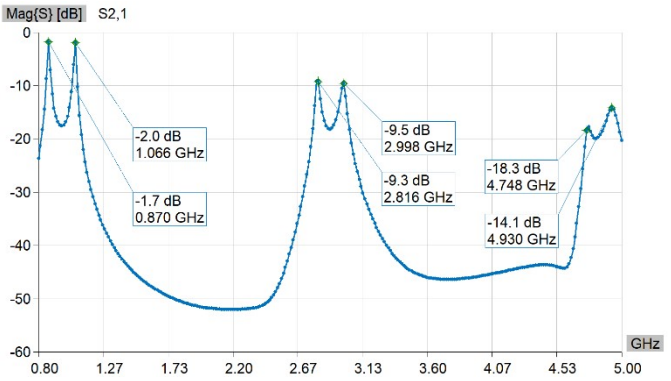

Fig. 6. Insertion loss response in frequency range 0.8 GHz – 5 GHz.

C. Coupling Curve Results

In case of both methods, models were re-simulated for different values of spacing between resonators, from range 0.1 mm to 10 mm. For each point, the equation (10) is calculated by inspecting resonances from MS graph and *s*-parameters. Results are overlaid on graph shown in Fig. 7,

where "MS" denotes CMA based method, while "s_{21}" denotes the method based on insertion loss response.

The graph from Fig. 7 confirms that these two approaches result in the same coupling coefficient curves, and it can be said the CMA based method is verified. Negligible differences could be reduced by additional increasing of EM simulation accuracy, which is for the purpose of this research considered unnecessary.

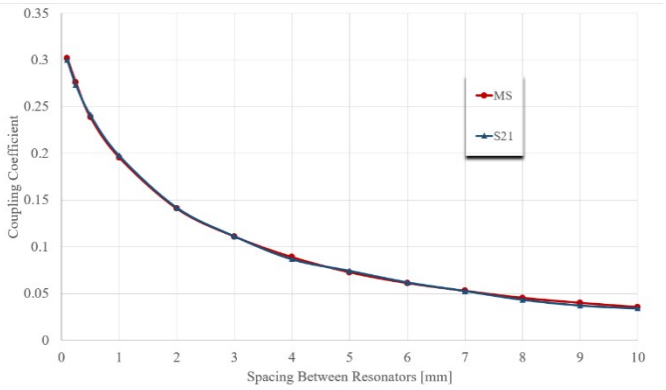

Fig. 7. Coupling curve in terms of spacing between resonators.

IV. Conclusion

In this paper, we have shown how CMA can be used in order to analyze resonant frequencies and coupling between resonators, and therefore can be used in bandpass microstrip filter synthesis. It provides very elegant solution to inspect internal resonances without taking care of feeding network and its potential influence. The validity of the results is confirmed with those obtained by inspecting *s*-parameters of the equivalent model with ports and feed lines.

Acknowledgment

This work was supported in part by the Ministry of Education, Science and Technological Development of the Republic of Serbia and by the Innovation Fund from the budget of the Republic of Serbia from the division of the Ministry of Education, Science and Technological Development, through the Serbia Competitiveness and Jobs Project (loan agreement with the World Bank).

References

[1] M. Dishal, "Alignment and Adjustment of Synchronously Tuned Multiple-Resonant-Circuit Filters," *Proceedings of the IRE*, vol. 39, no. 11, pp. 1448-1455, Nov. 1951.

[2] M. Dishal, "A Simple Design Procedure for Small Percentage Bandwidth Round-Rod Interdigital Filters (Correspondence)," *IEEE T. Microw. Theory*, vol. 13, no. 5, pp. 696-698, September 1965.

[3] R. J. Garbacz, R. H. Turpin, "A generalized expansion for radiated and scattered felds", *IEEE T. Antenn. Propag.* vol. 19, no. 3, pp. 348-358, 1971.

[4] Q. Wu, "Characteristic Mode Assisted Design of Dielectric Resonator Antennas With Feedings," *IEEE T. Antenn. Propag*, vol. 67, no. 8, pp. 5294-5304, 2019.

[5] J. J. Borchardt and T. C. Lapointe, "U-Slot Patch Antenna Principle and Design Methodology Using Characteristic Mode Analysis and Coupled Mode Theory," *IEEE Access*, vol. 7, pp. 109375-109385, 2019.

[6] L. Guo, J. Zhao, C. Wang, Y. Chen and S. Yang, "Scattering Control Using Advanced Characteristic Mode Theories," *2018 IEEE Int. Symp. Antenn. Propag. & USNC/URSI Nat. Radio Sci. Meeting*, 2018, pp. 1127-1128.

[7] Z. Xu, S. Li, Y. Liu, H. Zhao and X. Yin, "Characteristic Mode Analysis of Complex Spoof Localized Surface Plasmon Resonators," *IEEE Access*, vol. 6, pp. 2871-2878, 2018.

[8] R. F. Harrington, J. R. Mautz, "The Theory of Characteristic Modes for Conducting Bodies," *IEEE T. Antenn. Propag.*, vol. 19, no. 5, pp. 622-628, 1971.

[9] WIPL-D Pro CAD 2020, WIPL-D d.o.o, Belgrade, 2020.

[10] R. Harrington, J. Mautz, Yu Chang, "Characteristic modes for dielectric and magnetic bodies," *IEEE T. Antenn. Propag.*, vol. 20, no. 2, pp. 194-198, March 1972.

[11] J.-S. Hong, "Couplings of asynchronously tuned coupled microwave resonators," *IEE P. – Microw. Anten. P.*, vol. 147, no. 5, Oct. 2000, pp. 354–358.

[12] J.G. Hong, *Microstrip Filters for RF/Microwave Applications,* 2nd ed. Hoboken, New Jersey: Wiley, 2011.